MEMS-Based Wearable Eyeglasses for Eye Health Monitoring

doi: 10.1088/2057-1976/ab562e

MEMS- Based Wearable Eyeglasses for Eye Health Monitoring

Neelam Kaushik[1*], Takashi Sasaki[1], Yoshiki Takahashi[1], Toru Nakazawa[2] and Kazuhiro Hane[1]
[1]*Department of Fine mechanics., Tohoku University, Sendai, Japan*
[2]*Graduate school of Medicine, Tohoku University, Sendai, Japan*
[*]*Corresponding author: neelam@hane.mech.tohoku.ac.jp*

Abstract

A large number of world population suffer from vision related diseases/defects. Visual health supervision is important for detection, prevention and treatment of eyes disorders. Images of retina/fundus are important for diagnosis of eye diseases. In this paper we report on design and development of a wearable eyeglass type retinal imaging system using a 2D MEMS scanner for ocular health monitoring. Several wearability criteria for instance weight and size factor should be taken into account while designing a wearable health monitoring system. The 2D-MEMS scanner used in the system is small in size, that helps to fabricate an easy to use and lightweight wearable imaging device. The net weight of fabricated system including optical components is 150 grams. Sensitivity of the system was estimated by measuring the signal-to-noise ratio for high and low reflectance materials. Signal-to-noise ratio was 7 for high reflectance material and about 4 for biological samples. Imaging results were obtained by scanning a model eye, ham slice and enucleated swine eye in real time by custom made LabVIEW program. The fabricated system has adequate sensitivity and resolution for the observation of retinal arteries and optic disc for detection of eye diseases.

1.Introduction

Development of wearable devices for health monitoring has gained a lot of attention in the scientific community and industry in past few years [1-3]. As world population is ageing and costs of healthcare is increasing, there is a need to monitor patient's health status in his/her personal environment and provide access to healthcare for as many people as possible [4]. The focus is on shifting the healthcare expenditures from treatment to prevention. Wearable devices will have a significant impact on the practice of medicine since they fulfill the critical need for a technology than can enhance the quality of life while reducing healthcare cost.

A variety of system prototypes and commercial products have been produced in the recent years which aims to provide real time feed-back information about one's health condition, either to user itself or to a medical center. Wearable systems for health monitoring contain various types of sensors that are capable of measuring important physiological parameters like heart rate, body temperature, blood pressure, electrocardiogram etc. [5-7]. A recent addition to wearable devices is smart glasses that are used in many ways such as recording, streaming video, data transmission, telemedicine and can provide augmented or virtual reality in addition to wearer's environment [8]. There are varieties of smart glasses and health monitoring devices but none of them works for imaging of eye. Eye related diseases and defects have an enormous adverse effects on human health, efficiency and social welfare. Many retinal diseases remain undetected until permanent vision loss or damage occurs because they are asymptomatic in early stages and eye examining is limited due to limited access to expensive specialized equipment and field experts. Eye screening for large population for an extended period of time is not only expensive but also time consuming. As a result, diagnostics are passive and disease is noticed only when it shows some symptoms. Long term monitoring can help in early detection of vital signs and timely prevention of some

vision problems [9-10]. One method of early detection of eye diseases is regular monitoring of eyes by use of instrument eyeglasses or wearable smart glasses to collect images of retina/fundus. Therefore, it is necessary to develop an eyeglass type wearable retinal imaging device that can provide regular monitoring of eyes.

In this paper we report on design and fabrication of wearable eyeglasses using a 2D - MEMS scanner for retinal imaging. MEMS scanner can facilitate fabrication of wearable devices as they are small, light in weight, cost effective, allow miniaturization in addition to low power consumption per scan axis. They also provide multi-dimensional scan capabilities even for smaller areas. Confocal scanning microscope using MEMS devices is emerging as a new imaging technology for in vivo and ex-vivo imaging of internal organs [11-12]. 2D- MEMS scanners are alternatively used in place of galvanometer scanners for various optical coherence tomography systems [13-14]and portable scanning laser scanning systems [15]. Recently there are some wearable products such as retinal imaging laser eyewear developed by (QD Laser, Japan) which uses MEMS mirror and a tiny projector for directly projecting images on the retina. These eyeglasses are being developed for people with low vision and purpose is projection of images [16,17,18], but detection of reflectance from retina is not reported yet. The usage of a laser to illuminate the eye and detection of reflection from retinal surface through a detector makes our smart glass different from projection glasses. The purpose of this work is to fabricate a low cost, easy- to- use, and unobtrusive wearable eyeglass device that can take retinal images and help patients to check the eyes at home on a regular basis to avoid eye disorders, furthermore for person suffering from known diseases can be under constant monitoring.

2. Design and Experimental set-up

The schematic of fabricated wearable smart glass type retinal imaging system is shown in figure 1(a). The incident light path is shown in blue color and reflected signal path is represented in red color. The imaging system consists of a 2D MEMS scanner, glass type relay optics and detector. A 638nm laser diode was used for illumination. The laser beam was collimated by collimating lens with a focal length of 2.0 mm by using a single mode optical fiber. The collimated beam had a 0.38mm($1/e^2$) diameter and it was reflected from a 2D MEMS scanner and focused on the retina by glass type relay optics. An achromatic lens (L1) with focal length of 12.5mm was used to focus laser beam into glass type relay system. Figure 1(b) shows the prototype of the fabricated wearable eyeglass type imaging system with 2D MEMS scanner. Figure 1(c) shows the wearability of the fabricated device. The fabricated system was not used to take images from human retina.

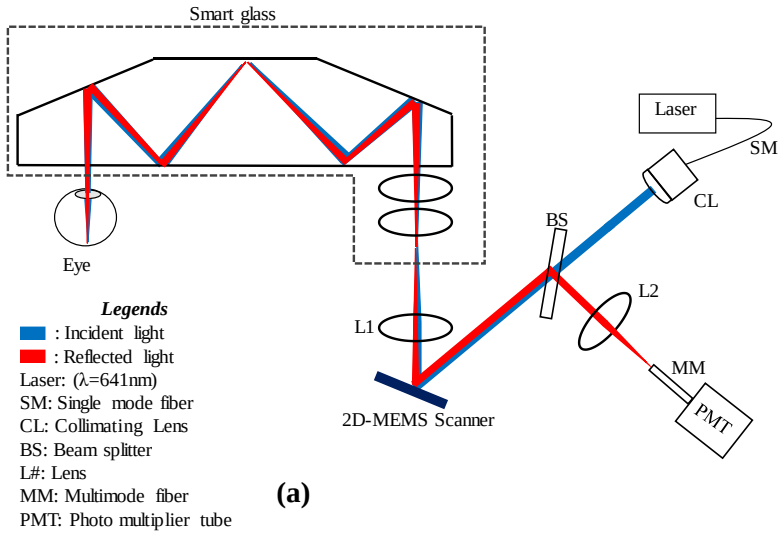

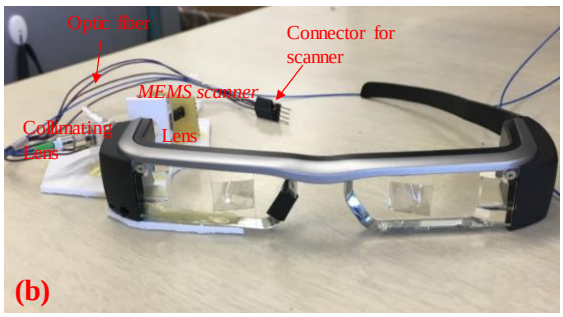

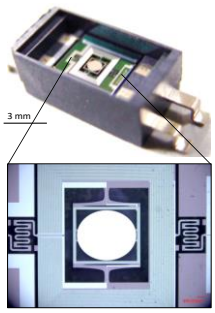

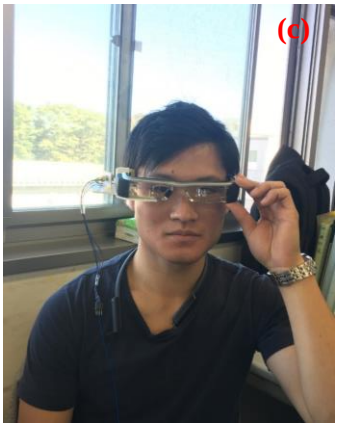

Figure1: (a) Schematic of fabricated wearable eyeglass type retinal imaging system, (b) photograph of actual system showing 2D-MEMS scanner used for scanning. (c) shows wearability of the fabricated system. For the publication purpose, consent was obtained from the participant of figure 1(c).

The 2D-MEMS scanner [model no. S12238-01P(X), Hamamatsu Photonics, Japan] used in the system is approximately 0.9mm in diameter. MEMS scanner had 22.5kHz and 680Hz resonant frequencies in X and Y axes. The MEMS scanner was controlled by a custom made driving circuit. For glass type relay optics, a commercially available smart glass (Epson Moverio, BT200) was used. Epson glass was modified to make it suitable for retinal imaging. Original projection system of smart glass was converted into detection system by replacing the LCD panel with our designed optics including MEMS scanner. The reflected signals from retina were detected by a photomultiplier tube (PMT) (H10721-20, Hamamatsu Photonics, Japan) through a pinhole. For the confocal pinhole a multimode optical fiber with a core diameter of 50μm was used. The focal length of collection lens (L2) was 12mm. The detected signals were low pass filtered with a cut off frequency of 1MHz in order to avoid aliasing artifacts in the image. The 2D image of retina was obtained by changing the scan angle of MEMS scanner. The detected signals were acquired by using a 12-bit PCI card (AI-1204Z- PCI, Contec. Co., Ltd. Japan). Custom software developed using LabVIEW was used for real time display of images obtained by the smart glass set-up. Figure 1(b) is the photograph of actual system showing 2D MEMS scanner. The weight of wearable glass including MEMS scanner and other optical components is about 150 grams so it is lightweight device. To characterize the imaging performance of the fabricated system we used a commercially available imaging model eye (OEMI-7), and it is the most realistic eye model for ocular fundus imaging. It has an anterior chamber, crystalline lens and fundus. The eye was filled with water before measurement to completely mimic the human eye. For biological samples a thin ham slice and enucleated swine eye were used. The enucleated swine eyes for the experiment were bought

from Sendai Central meat whole sale market Co. Ltd. For experiments using animal parts we followed the regulations specified by Tohoku University. The measured laser intensity in front of model eye was much smaller than the maximum permissible beam power recommended by the American National Standards Institute.

3. Results and discussion

Capabilities of our fabricated system for its application in wearable devices were determined by examining some important parameters such as resolution, sensitivity and imaging properties. Safe exposure during retinal imaging should be considered while designing an optical system that uses laser for illumination. We calculated maximum permissible beam powers for thermal and photochemical exposure for our fabricated system. Results from experiments are explained in following subsections.

3.1 Resolution

Resolution of the fabricated system was estimated by measuring the modular transfer function of complete system and also by using a 1951 USAF resolution test target as model retina. The quality of an optical system can be determined by modular transfer function (MTF), which is the Fourier transform of the point spread function (PSF) [19]. Therefore, the spatial resolution can be calculated from the high frequency profile of the MTF. The MTF plot is expressed in the terms of spatial frequency (lines/mm or cycles/mm) on the x-axis and modulation (contrast) on the y-axis. The actual resolution is always different from the theoretical values as the total resolution of system is dependent on all the components used in the system. The resolution of real images depends on many experimental aspects such as mechanical drift or sample deformation. So the resolvability of real images should be estimated not only from optical theory but also from the

image itself. The main and simple method for calculating MTF is to determine the PSF and then transform it into MTF. We calculated the MTF of our system from laser spot obtained at the retinal plane. The PSF of the laser spot was extracted using the Image J software. The MTF of the entire system was calculated by the Fourier Transform of PSF. PSF obtained from the laser spot at the

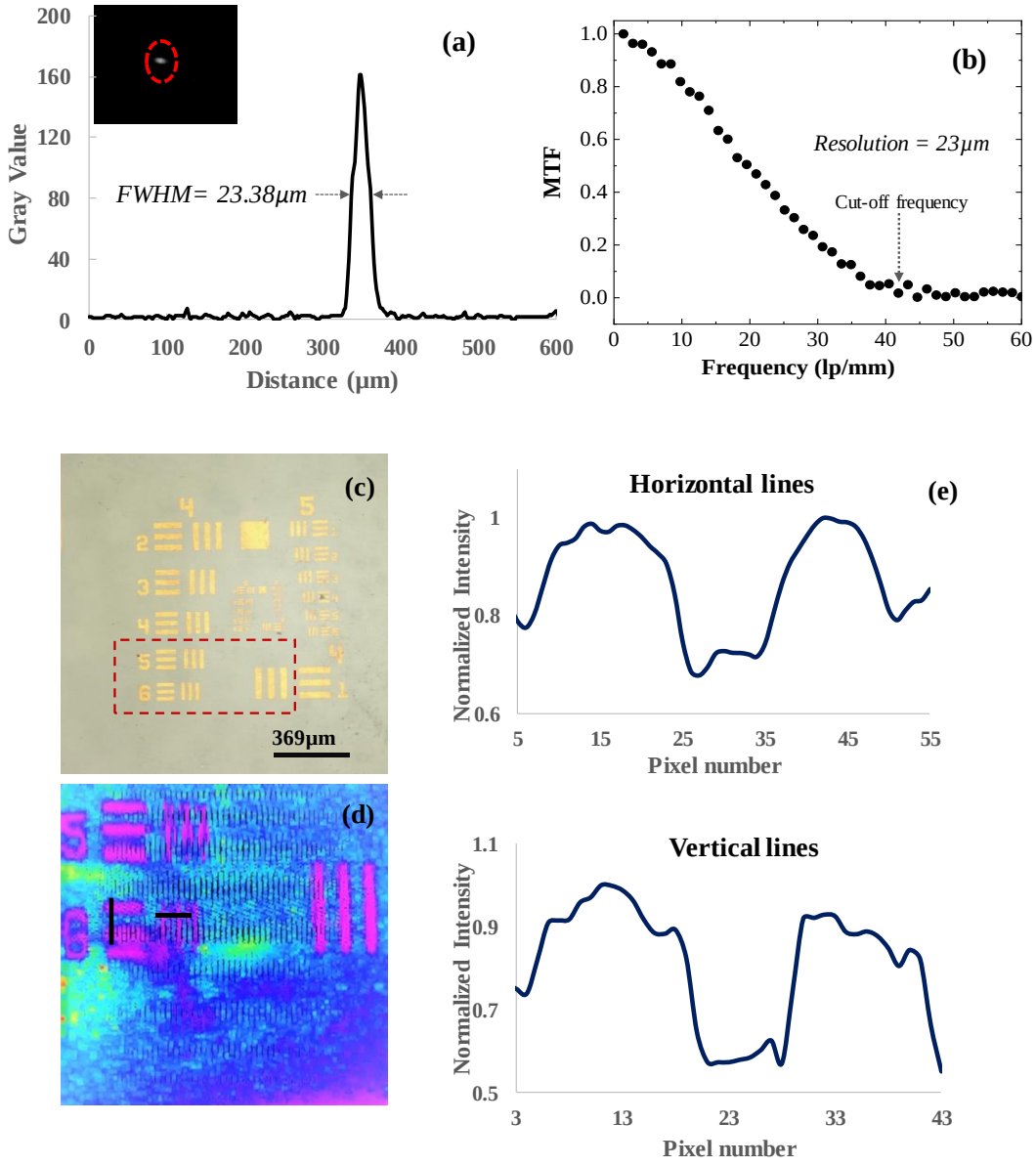

Figure 2: (a) PSF of the actual system at the retinal plane. Inset of figure 1(a) is the CCD camera image of laser spot. (b) MTF of the complete optical system calculated from PSF of the system. The black curve represents the actual MTF of the system on the retinal plane. (c) Optical

microscope image of group 4 and 5 of a 1951 USAF resolution target. (d) Reflectance of image patterns marked in the scan area of fig2 (c). (e) cross section from horizontal and vertical lines of fig 2(d) marked by black lines.

retinal plane is shown in figure 2(a), which is narrow, (full width at half maxima FWHM, value is 23.38μm) which means imaging performance is good. Inset of figure 2(a) is the CCD camera image of actual laser spot obtained at the retinal plane. Figure 2(b) is the MTF graph which shows the contrast (modulus of OTF) in the image as a function of frequency at nominal focus. The black curve represents the MTF of actual system at the center. The measured MTF shows a resolution of 23μm which is calculated from cut-off spatial frequency. Figure 2(c) is the optical microscope image of resolution test target showing group 4 and 5. The area marked by dashed line is the scanned area for group 4 element 5 and 6. Reflectance image obtained by scanning is shown in fig2(d). Cross-section from the area indicated by black lines in fig2(d) is shown in 2(e). The smallest line pairs that could be resolved by our system were group 4 element 6, which corresponds to a lateral resolution of 35μm. For evaluation, the size of main retinal arteries is about 200μm and the small capillaries in the eye are about the size of 10μm to 20μm, the optic disc of human eye is about 1.5mm so our system have enough resolution for imaging retinal arteries and optics disc. Optic disc images can be used for basic diagnosis of eye related disorders such as glaucoma. We also calculated total resolvable spots for our fabricated system with respect to scanning area of MEMS scanner. The number of resolvable sports determine the relationship between field of view and resolution of any scanning system. The resolvable spots can be calculated by scanning mirror diameter d_m and optical scan angle $\pm\Theta_m$. The diffraction angle for the focused Gaussian beam in relation of mirror diameter can be written as

Θ_{diff} =$\tan^{-1}$[2.45*($\lambda_0/\pi d_m$)], where λ_0 is the center wavelength used in the system. The resolvable spots for the scanning system can be calculated by the ratio of total scanning angle and two times of diffraction angle:

Total resolvable spots = 2 Θ_m/2 $\Theta_{diff.}$

The diameter of MEMS scanner was 1mm and we used ±5.0^o optical scanning angle for all the measurements at 638nm. Theoretically the total resolvable spots would be 176. The incident beam on the cornea was 0.38mm($1/e^2$) resulting in a spot size of 36μm ($1/e^2$ diameter). The scan length on the retina was 6mm. The number of resolvable spot by using these measured parameters is calculated by dividing the total scan length by spot size diameter. The calculated resolvable spots are 167 which are close to the theoretical value.

3.2 Signal-to-Noise Ratio

The reflectance signal from biological tissues is not very high in the visible range wavelength, so it is important to check the sensitivity of the system by calculating the signal to noise ratio. In our fabricated system image is acquired by using an analog-to-digital converter that digitalizes the analog output of photodetector, and experimentally estimation of exact amount of noise from pixelated image is challenging. Considering these facts, the sensitivity of the system was checked by obtaining reflectance signal from different samples with variant reflectivity such as metal pattern, a model eye filled with water and biological sample such as a thin ham slice. For biological sample the ham slice was selected as it is readily available and easy to test. The control voltage of the photomultiplier for the measurement was 0.75V. Figure 3(a) shows the picture of patterned metal sample used for the measurement. Reflectance signals were obtained from scan area marked by square in dotted lines on Fig 3(a). Bright strips in figure 3(b) represents metal pattern with high

reflectance, the SNR ratio for metal sample was 7 and base is resin with low reflectance with a SNR of 3. Fig 3(c) is the photograph of model eye and 3(d), (f) are the CCD camera images of the retina of model eye. Figure3(e) and 3(g) are the reflectance images of different scan areas on the retina of model eye. The ring like pattern in figure 3(e) is the bubble like pattern on the retina of model eye. These bubble like patterns in the model eye represents foreign body inside of eye. The bright colored pattern in 3(g) is the optic disc of model eye marked in square scan area in camera image. The SNR for model eye was 5. Figure 3(h) is the photograph of whole muscle ham sample. This type of meat is usually most homogenous in terms of microstructures. Reflectance signal were obtained from a scan area marked by square in the dotted lines on figure 3(h). Bright colored spots in figure 3(i) represents the tissues with high reflectance and light contrast base represents the tissues with low reflectance. These are basically starch grains in protein matrix [20]. The measured SNR for ham slice was 4. The smart glass used in the system is a projection type of glass and it is not designed for detection application. There is loss of light intensity through the glass surfaces of the smart glass but the reflectance signals could be detected with added optics. For imaging, a minimum signal to noise ratio of 3 is recommended [21]. The signal to noise ratio for all the samples with our fabricated device was more than 3 so it is adequate for imaging.

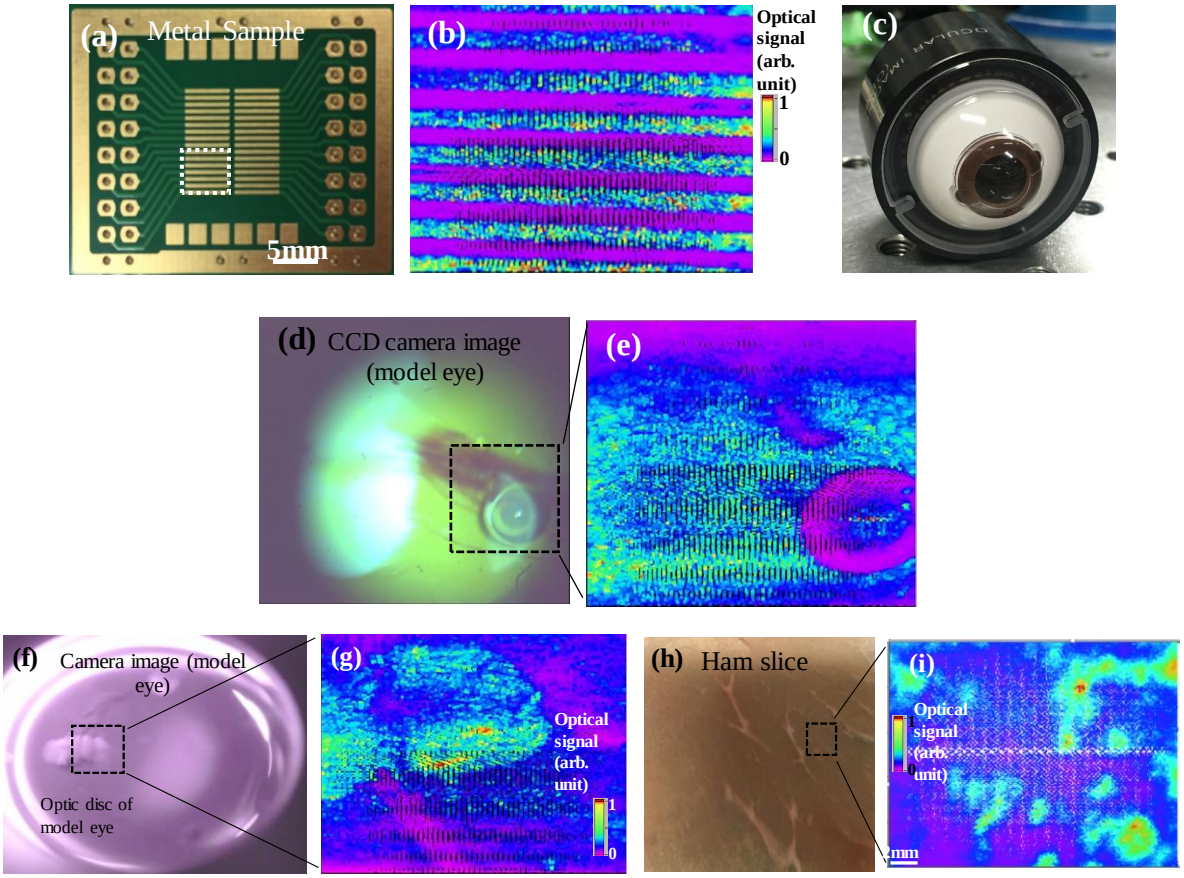

Figure 3: (a) Photo of metal sample. The dotted square marked on the photo shows the scan area used for imaging. (b) reflectance image obtained by scan area marked on metal sample. (c) photograph of model eye. (d), (f) CCD camera images showing the scan area on the retina of model eye. (e), (g) Reflectance image obtained by scanning the area marked on figure (d) and (f). (h) Photograph of ham slice. (i) Reflectance image obtained by scanning the marked area of fig (h).

The fabricated system is capable of imaging the sample with very low to high reflectance and signal intensity increased with increase in gain control voltage of the photomultiplier tube. The results from the fabricated system shows enough sensitivity to image biological tissues. The imaging performance can be further improved by reducing the noise in the system. For image acquisition and background subtraction we developed custom software in LabVIEW (National Instruments, Austin, Texas). The images were corrected in real time for background noise removal

without object i.e. under no reflection from object. Figure 4(a) shows the CCD camera image of custom made model eye. The scan area covers the optic disc of the model eye which is marked with dotted square. Figure 4(b) is image acquired without using noise removal program and 4(c) is image taken using noise removal program. A clear difference between two reflectance images with and without noise can be observed.

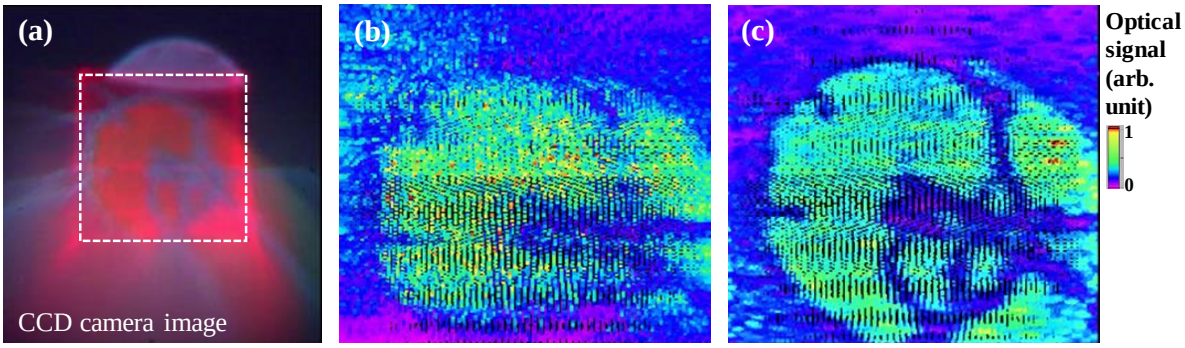

Figure 4: (a) CCD camera image of model eye showing the scan area. (b) Image of model eye acquired without using noise removal program. (c) Image of model eye acquired using noise removal program.

3.3 Imaging

The field of view (FOV) of eyeglass type system calculated from the measurement was 16^{o} in horizontal axis and 13^{o} in vertical axis. The imaging speed was 88 frames per second(fps)with 500 lines per frame. The imaging speed can be altered depending on experimental conditions. For image acquisition we used custom software in LabVIEW. An enucleated swine eye was used for further imaging. As human retinal tissues loses histological and optical properties quickly after death, pig eye was chosen as it is readily available for experiments. Additionally, besides its size, numerous features are similar to those of human eye.

Figure 5(a) is the photograph of enucleated swine eye used for the imaging. The pupil size of the enucleated swine was 10mm. Figure 5(b) and (c) are the CCD camera images showing the scan area by dotted squares on the retinal surface of enucleated swine eye. Reflectance signal obtained by scanning swine eye are shown in figure 5(d) and 5(e). The bright contrast patterns in both the images represent the blood vessels on the retina surface. There is slight variation in the CCD camera image and reflectance image obtained by scanning of enucleated swine eye.

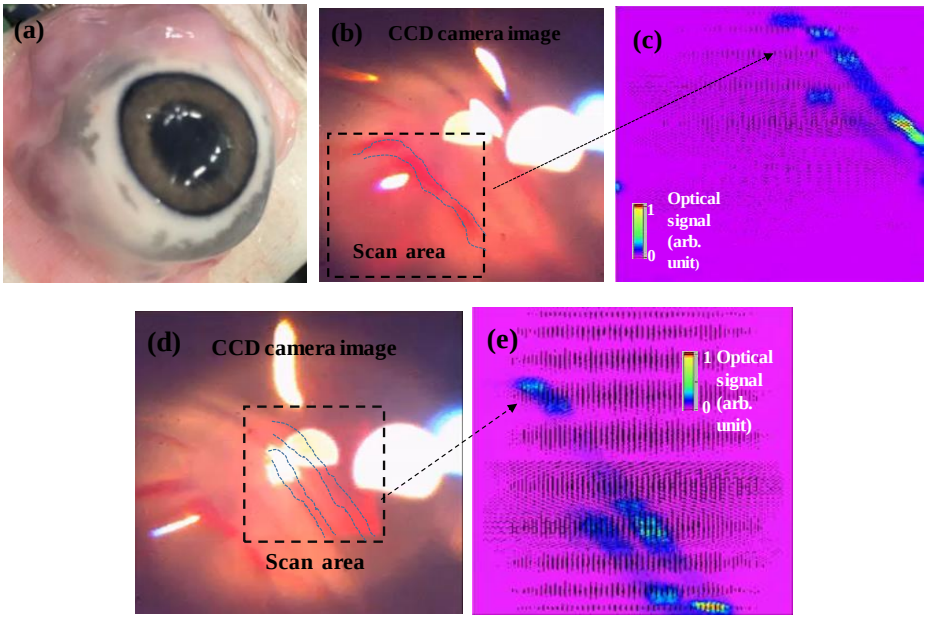

Figure 5: (a) Photograph of enucleated swine eye. (b) and (d) are CCD camera image of retina of enucleated swine eye. (c) and (e) reflectance signal from retina of enucleated swine eye.

The reason for variation is that there are several factors that influence the appearance and size of retinal vessels as a function of wavelength. The most important factor is optical absorption by blood columns and vessels, as they have low contrast against fundus background for wavelengths longer than 600nm [22]. In the vessels where blood thickness is greater absorption is high and

where blood thickness is low, transmission is high. The reflectance image of blood vessels looks broken in some places due to difference in blood volume in vessels compared to CCD camera image. The reflectance signal from biological sample is not so high compared to metal sample, but imaging was possible even for samples with low reflectance. These results demonstrate that the eyeglass type system which is fabricated by using a commercially available smart glass designed only for projection is capable of imaging biological samples with our designed optics and can be used for retinal imaging.

3.4 Safe use of wearable device

Optical devices that are used for imaging of retina often brings light into the eye through the pupil.

Retinal damage from light exposure occurs principally from three different ways, (1) thermal damage, (2) photochemical damage and (3) thermo-acoustic damage. The literature about the scanning laser system often report about the details of laser power used which is generally below the safely limits recommended by American National Standards Institute's (ANSI) laser safety standards [23]. These standards are about the use of maximum laser power and maximum permissible exposure over a certain pupil area for safety of patients. There is no perfect method to evaluate the potential hazard from the retinal exposure in system using laser scanning. We should first check the static beam power in front of the eye. In our fabricated system the laser power of static beam used for the experiments was 10μW which is quite low. We calculated the maximum beam power for our eyeglass type system by considering the visual angle for an exposure of 5minutes (300s). A continuous wave laser with 638nm wavelength was used. The maximum permissible $MP\Phi_B$ (in watts) beam power for thermal limits was calculated by using the following expression [24]:

$$MP\Phi_{B,\,CW,\,th} = 1.41\ X\ 10^{-4} C_T P^{-1} 300 \alpha_F$$

Where C_T is function of wavelength and it is 1 for λ (400-700) [19]. P is pupil function which is defined by wavelength and exposure time. The exposure time was 300s which is reasonable duration for most clinical and experimental situations. The visual angle (α_F) was 87.5mrad and calculated value for thermal limit is 0.6773 Watts.

The photochemical limits in watts can be calculated by following expression [24]:

$$MP\Phi_{B,\,CW,\,ph} = 2.36\ X\ 10^{-8} C_B \alpha_F^{\,2}$$

C_B = is function of wavelength and it is 1000 for λ>600nm [24]. The calculated value for photochemical limit is 0.180 watts. The measured laser intensity in front of model eye is much lower than the calculated maximum permissible beam power limits for thermal and photochemical damage and it is safe for use.

Conclusions

In summary, a wearable eyeglass type retinal imaging system was fabricated using a 2D MEMS scanning mirror and a commercially available projection smart glass. With added designed optics, the projection smart glass was able to detect reflectance signal from samples with variable reflectance. The images from model eye and biological samples such as ham slice and swine eye were successfully obtained. The wearable glass type retinal imaging system is lightweight measuring 150 grams. 2D-MEMS scanner helped to reduce system size and weight with advantage of fast scanning. The proposed wearable eyeglass type system can be applied an easy to use screening and regular monitoring tool for imaging of eye. The fabricated system has enough resolution for early detection and diagnosis of eye diseases such as glaucoma. The results are encouraging for development of wearable imaging device for eyes.

References

1. L. Gatzoulis and I. Iakavidis, “Wearable and portable eHealth systems”, IEEE Eng. Med. Biol. Mag, **26** (5),51(2007).
2. A. Lymperis and A. Dittmar, “Advanced wearable health systems and applications, research and development efforts in the European Union”, IEEE Eng. Med. Biol. Mag, **26**,29(2007).
3. G. Troster, “The agenda of wearable healthcare”, IMIA Yearbook of Medical Informatics. Stuttart, Germany: Schattauer,**125** (2005).
4. Y. Hao and R. Foster, “Wireless body sensor networks for health-monitoring applications”, Phys. Meas. **29**, R27(2008).
5. O. O. Ogunduyile, K. Zuva, O. A. Randle, and T. Zuva, “Ubiquitous healthcare monitoring system using integrated triaxial accelerometer, S_PO_2 and location sensors”, Int. J. UbiComp, **4** (2), 1(2013).
6. P. Bonato, “Wearable sensors and systems”, IEEE Eng. Med. Biol. Mag., **29**, 25(2010).
7. Mary M. Rodgers, V.M. Pai and R.S. Conroy, “Recent advances in wearable sensors for health monitoring”, IEEE sensors Journal,**15**,3119 (2015).
8. S. Mitrasinovic, E. Camacho, N. Trivedi, J. Logan, C. Campbell, R. Zilinyi, B. Lieber, E. Bruce, B. Taylor, D. Martineau, E. L.P. Dumont, G. Appelboom and E.S. Connolly Jr., “Clinical and surgical applications of smart glasses”, Technology and health care **23**,381 (2015).
9. S. Rowe, C.H. MacLean and P.G. Shekelle, “Preventing visual loss from chronic eye disease in primary care: scientific review”, JAMA **291**(12)**,**1487(2004).

10. E.Y. Wong, J.E. Keeffe, J.L. Rait, H.T. Vu, A. Le, C. McCarty and H.R. Taylor, "Detection of undiagnosed glaucoma by eye health care professionals", Ophthalmology **111** (8),1508(2004).
11. H. Shin, M.C. Pierce, D. Lee, H. Ra, O. Solgaard, R. Richards-Kortum, "Fiber-optic confocal microscope using a MEMS scanner and miniature objective lens", Opt. Express **15**, 9113 (2007).
12. C.L. Arrasmith, D.L. Dickensheets, A. Mahadevan-Jansen, "MEMS-based handheld confocal microscope for in-vivo skin imaging", Opt. Express **18**, 3805 (2010).
13. K. H. Kim, B. H. Park, G. N. Maguluri, T. W. Lee, F. J. Rogomentich, M. G. Bancu, B. E. Bouma, J. F. de Boer, and J. J. Bernstein, "Two-axis magnetically –driven MEMS scanning catheter for endoscopic high- speed optical coherence tomography", Opt. Express. **15**, 18130 (2007).
14. D. Wang, L. Fu, X. Wang, Z. Gong, S. Samuelson, C. Duan, H. Jia, J. S. Ma, and H. Xie, "Endoscopic swept source optical coherence tomography based on a two-axis microelectromechanical system mirror", J. Biomed. Opt. **18**, 086005 (2013).
15. N. Kaushik, T. Sasaki, T. Nakazawa and K. Hane, "A simple retinal imaging system using a MEMS scanning mirror", Optical Eng.**57**,095101(2018).
16. https://journal.jp.fujitsu.com/en/2016/12/13/01/
17. https://www.qdlaser.com/en/applications/eyewear.html
18. https://www.nedo.go.jp/hyoukabu/articles/201805qd/pdf/201805qd.pdf
19. J.W. Goodman, "Introduction to Fourier Optics", 2nd edition, McGraw-Hill company, INC, (1996).
20. M. Pospiech, B. Tremlova, Z. Javurkova, "The microstructure of whole-muscle meat products", http://www.maso-international.cz/download/155_160_022015.pdf

21. R.H. Webb and G.W. Hughes, “Detectors for scanning video imagers”, Applied Optics 32,6227(1993).

22. R. Park, K. Twietmeyer, R. Chipman, N. Beaudry and D. Salyer, “Wavelength dependence of the apparent diameter of retinal blood vessels”, Applied Optics 44,1831 (2005).

23. ANSI, “American National Standard for safe use of lasers (ANSI 136.1),” ANSI 136.1-2000(The laser Institute of America,2000).

24. F.C. Delori, R.H. Webb, D. H. Sliney, “Maximum permissible exposures for ocular safety (ANSI 2000) with emphasis on ophthalmic devices,” J. Opt. Soc. Am. A, 24(5),1250-1265 (2007).